# Calculation of Hypersonic Flow over Bodies of Revolution at Small Angles of Attack

JOHN V. RAKICH*
*NASA Ames Research Center, Moffett Field, Calif.*

**A method-of-characteristics computer program is used to study the first-order effects of angle of attack on the flow about bodies of revolution moving through air at speeds for which real-gas effects arising from dissociation and ionization need to be considered. First-order perturbations of the surface pressure, density, enthalpy, and crossflow velocity are presented for several body shapes to illustrate differences between perfect-gas and equilibrium real-gas flows. The body shapes considered are pointed cones, a pointed ogive, and a spherically tipped cone. Ambient conditions correspond to those at 100,000-ft alt. Flight velocities range from 5000 to 75,000 fps for the pointed cones; ogive and sphere-cone results are presented for 20,000 fps flight velocity.**

## Nomenclature

$a$ = speed of sound
$h$ = enthalpy
$M$ = Mach number
$p$ = pressure
$r$ = radial coordinate, cylindrical coordinate system
$R$ = radial distance to shock wave
$R_b$ = nose radius for blunt-nosed body
$S$ = entropy
$u$ = velocity component in $x$ direction
$v$ = velocity component in $r$ direction
$\mathbf{V}$ = velocity vector
$V$ = scalar magnitude of velocity vector $\mathbf{V}$
$w$ = velocity component in circumferential direction (crossflow velocity)
$x,y,z$ = rectangular coordinates
$s,n,t$ = streamline coordinates
$\mathbf{s},\mathbf{n},\mathbf{t}$ = unit vectors, streamline coordinates (see Fig. 1)
$\alpha$ = angle of attack, rad
$\beta$ = $(M^2 - 1)^{1/2}$
$\xi$ = left-running characteristic coordinate
$\theta$ = flow angle measured from $x$ axis in meridional plane, $\tan^{-1}(v/u)$
$\eta$ = right-running characteristic coordinate
$\rho$ = density
$\sigma$ = shock-wave angle measured from $x$ axis
$\varphi$ = crossflow angle, $\sin^{-1}(w/V)$
$\Phi$ = azimuthal coordinate, cylindrical coordinate system
$\omega$ = ray angle, conical flow, $\tan^{-1}(r/x)$
$\omega_c$ = cone half-angle
$(\ )'$ = coordinates fixed with respect to the body (quantities presented in Figs. 4–8 are referenced to body axes)

### *Subscripts*

0 = zero-order variable from solution of axisymmetric, zero angle of attack flow
1 = first-order perturbation variable, implies a derivative with respect to $\alpha$ which is a function of $x$ and $r$ only, as defined by Eqs. (8)
$\alpha$ = first-order perturbation variable, implies a derivative with respect to $\alpha$ which is a function of $x$, $r$, and $\Phi$, as defined by Eq. (6)
$\infty$ = freestream conditions
$S$ = conditions immediately behind the shock wave
$B$ = conditions on the body
$cp$ = center of pressure
$m$ = coordinates fixed in the meridional plane

Presented as Preprint 64-430 at the AIAA 1st Annual Meeting, Washington, D. C., June 29–July 2, 1964; revision received November 20, 1964.

* Research Scientist. Member AIAA.

## Introduction

FLIGHT of aircraft and missiles at hypersonic speeds has created a need for re-examining existing methods of computing flow fields with emphasis on the real-gas effects arising from dissociation and ionization. In many cases of practical interest, the dominant features of a real-gas flow can be obtained by assuming the gas to be in equilibrium with respect to these processes, that is, in thermodynamic equilibrium. Numerous investigations have been made for axisymmetric flows of an equilibrium gas for both blunt-nosed and pointed bodies.[1–5] However, for asymmetric three-dimensional flows theoretical studies have, for the most part, been restricted to the usual perfect gas idealization. This paper illustrates some of the effects which result from including equilibrium thermodynamic properties in the calculation of supersonic flow over selected bodies of revolution at small angles of attack. The present work is, therefore, exploratory and is intended to determine what effects, if any, real-gas properties have on the surface pressure, density, and velocity.

Although the aircraft designer is invariably confronted with problems due to large angles of attack, it is nevertheless important to establish the initial slopes of the lift curve and other design parameters. Attention is, therefore, directed to the first-order perturbation problem that determines the rate of change of flow parameters at zero angle of attack. Use is made of a computer program based on a linearized method of characteristics. Such methods have recently been successfully used to calculate perfect-gas flows over yawed, spherically blunted and pointed bodies of revolution.[6,7] Brong and Edelfelt[6] derived perturbation equations applicable to equilibrium flow, but presented results only for a perfect gas. The equations given in Ref. 6 contain thermodynamic derivatives which, for a perfect gas, are expressible in terms of the gas constant and the specific-heat ratio. For a real gas, however, it is necessary to evaluate these derivatives numerically from tabular thermodynamic data. Present results are obtained with computer programs that include the pertinent thermodynamic derivatives. Solutions for pointed cones are used to illustrate the real-gas effects at varying flight velocities and for varying cone angles. Solutions for an ogival body and for a spherically tipped cone are also presented as examples of more complicated flows.

## Analysis

The equations and procedures given in Ref. 7 will be summarized and generalized here so as to allow for equilibrium gas properties. This review will first cover, briefly, the equations

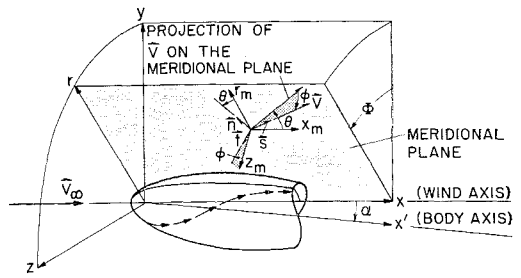


**Fig. 1 Coordinate systems.**

applicable to general bodies of revolution, and the corresponding relations for conical flow will then be outlined. Finally, the manner in which the gas properties enter these equations will be discussed.

### Equations for General Bodies of Revolution

The combined continuity and momentum equations are written in terms of streamline (intrinsic) coordinates $s,n,t$ as independent variables (see Fig. 1). These equations, which are linearized with respect to the crossflow angle $\varphi$ are

$$\frac{\beta^2}{\rho V^2}\frac{\partial p}{\partial s} + \frac{\partial \theta}{\partial n} + \frac{\partial \varphi}{\partial t} + \frac{\sin\theta}{r} = 0 \tag{1a}$$

$$\frac{1}{\rho V^2}\frac{\partial p}{\partial n} + \frac{\partial \theta}{\partial s} = 0 \tag{1b}$$

$$\frac{1}{\rho V^2}\frac{\partial p}{\partial t} + \frac{\partial \varphi}{\partial s} + \frac{\varphi \sin\theta}{r} = 0 \tag{1c}$$

The foregoing relations are supplemented by the conditions of constant entropy along streamlines

$$(\partial S/\partial s) = 0 \tag{2}$$

constant total enthalpy

$$h + (V^2/2) = H = \text{const} \tag{3}$$

and the equations of state

$$h = h(p,\rho) \tag{4a}$$

$$a = a(p,\rho) \tag{4b}$$

$$S = S(p,\rho) \tag{4c}$$

In order to determine the desired asymmetric flow field by the linearized characteristics method, it is first necessary to obtain from Eqs. (1–4) the analogous set of perturbation equations. The usual procedure is to substitute for all of the dependent variables expansions of the form

$$p(x,r,\Phi;\alpha) = p_0(x,r) + \alpha p_\alpha(x,r,\Phi) \tag{5}$$

where, for brevity, the subscript 0 is used to indicate a quantity obtained from the solution of the axisymmetric flow, and the subscript $\alpha$ is used to indicate the derivative

$$p_\alpha \equiv (dp/d\alpha)_{\alpha=0} \tag{6}$$

Also, it is necessary to express the partial derivatives with respect to $s,n,t$ in terms of the streamline coordinates of the axisymmetric flow $s_0,n_0,t_0$. This is done, to first order in $\alpha$, by the following formulas

$$\frac{\partial}{\partial s} = \frac{\partial}{\partial s_0} + \alpha\left(\theta_\alpha \frac{\partial}{\partial n_0} + \varphi_\alpha \frac{\partial}{\partial t_0}\right) \tag{7a}$$

$$\frac{\partial}{\partial n} = \frac{\partial}{\partial n_0} - \alpha\theta_\alpha \frac{\partial}{\partial s_0} \tag{7b}$$

$$\frac{\partial}{\partial t} = \frac{\partial}{\partial t_0} - \alpha\varphi_\alpha \frac{\partial}{\partial s_0} \tag{7c}$$

Finally, the problem is reduced to an axisymmetric one by the expansion of the dependent variables in a Fourier series in terms of the meridional angle $\Phi$. However, in the first-order yaw problem, it is necessary to retain only the first term of such an expansion.[8, 9] Thus the final perturbation variables take the form

$$\left.\begin{aligned} p_1(x,r) &= \frac{1}{\cos\Phi}\, p_\alpha(x,r,\Phi) \equiv \frac{1}{\cos\Phi}\left(\frac{dp}{d\alpha}\right)_{\alpha=0} \\ \theta_1(x,r) &= \frac{1}{\cos\Phi}\, \theta_\alpha(x,r,\Phi) \equiv \frac{1}{\cos\Phi}\left(\frac{d\theta}{d\alpha}\right)_{\alpha=0} \\ \varphi_1(x,r) &= \frac{1}{\sin\Phi}\, \varphi_\alpha(x,r,\Phi) \equiv \frac{1}{\sin\Phi}\left(\frac{d\varphi}{d\alpha}\right)_{\alpha=0} \end{aligned}\right\} \tag{8}$$

The crossflow velocity perturbation is obtained from the crossflow angle with the relation $w_1 = V_0\varphi_1$.

Substituting Eqs. (7) and (8) into Eqs. (1–4), one obtains the following set of perturbation equations:

Momentum and Continuity

$$\frac{\beta_0^2}{\rho_0 V_0^2}\frac{\partial p_1}{\partial s_0} + \frac{\partial \theta_1}{\partial n_0} = -\frac{1}{r}(\varphi_1 + \theta_1\cos\theta_0) - \left(\frac{\beta_0^2}{\rho_0 V_0^2}\frac{\partial p_0}{\partial n_0} - \frac{\partial \theta_0}{\partial s_0}\right)\theta_1 - \frac{1}{\rho_0 V_0^2}\frac{\partial p_0}{\partial s_0} \times \left(2\frac{V_1}{V_0} - 2M_0^2\frac{a_1}{a_0} - \beta_0^2\frac{\rho_1}{\rho_0}\right) \tag{9a}$$

$$\frac{1}{\rho_0 V_0^2}\frac{\partial p_1}{\partial n_0} + \frac{\partial \theta_1}{\partial s_0} = \left(\frac{1}{\rho_0 V_0^2}\frac{\partial p_0}{\partial s_0} - \frac{\partial \theta_0}{\partial n_0}\right)\theta_1 + \frac{1}{\rho_0 V_0^2}\frac{\partial p_0}{\partial n_0}\left(2\frac{V_1}{V_0} + \frac{\rho_1}{\rho_0}\right) \tag{9b}$$

$$\frac{\partial \varphi_1}{\partial s_0} = \left(\frac{1}{\rho_0 V_0^2}\frac{\partial p_0}{\partial s_0} - \frac{\sin\theta_0}{r}\right)\varphi_1 + \frac{p_1}{r\rho_0 V_0^2} \tag{9c}$$

Entropy

$$(\partial S_1/\partial s_0) = -\theta_1(dS_0/dn_0) \tag{10}$$

Total Enthalpy

$$h_1 + V_0 V_1 = 0 \tag{11}$$

State

$$h_1 = (\partial h/\partial p)_\rho\, p_1 + (\partial h/\partial \rho)_p\, \rho_1 \tag{12a}$$

$$a_1 = (\partial a/\partial p)_\rho\, p_1 + (\partial a/\partial \rho)_p\, \rho_1 \tag{12b}$$

$$S_1 = (\partial S/\partial p)_\rho\, p_1 + (\partial S/\partial \rho)_p\, \rho_1 \tag{12c}$$

The number of equations can be reduced to five if velocity and sound speed perturbations are eliminated with the use of Eqs. (11, 12a, and 12b). Also, for supersonic flow, Eqs. (9a) and (9b) can be simplified if the derivatives are projected onto the characteristic directions $(\xi,\eta)$ of the unperturbed flow with the formulas

$$\frac{\partial}{\partial s_0} = \frac{M_0}{2\beta_0}\left(\frac{\partial}{\partial \eta} + \frac{\partial}{\partial \xi}\right) \tag{13a}$$

$$\frac{\partial}{\partial n_0} = \frac{M_0}{2}\left(\frac{\partial}{\partial \eta} - \frac{\partial}{\partial \xi}\right) \tag{13b}$$

Using these transformations one can obtain the following compatibility equations, each of which contains derivatives in one direction only:

$$\frac{\beta_0}{\rho_0 V_0^2}\frac{\partial p_1}{\partial \eta} + \frac{\partial \theta_1}{\partial \eta} = F_1 - G \tag{14a}$$

$$\frac{\beta_0}{\rho_0 V_0^2}\frac{\partial p_1}{\partial \xi} - \frac{\partial \theta_1}{\partial \xi} = F_2 - G \tag{14b}$$

where the terms on the right side of the equations are

$$G = (\varphi_1 + \theta_1 \cos\theta_0)/M_0 r$$

$$F_1 = \frac{\beta_0}{M_0\rho_0 V_0^2}\left[(A + \theta_1)\frac{\partial p_0}{\partial s_0} - (B + \beta_0\theta_1)\frac{\partial p_0}{\partial n_0}\right] + \frac{\theta_1}{M_0}\left(\frac{\partial\theta_0}{\partial s_0} - \beta_0\frac{\partial\theta_0}{\partial n_0}\right)$$

$$F_2 = \frac{\beta_0}{M_0\rho_0 V_0^2}\left[(A - \theta_1)\frac{\partial p_0}{\partial s_0} + (B + \beta_0\theta_1)\frac{\partial p_0}{\partial n_0}\right] + \frac{\theta_1}{M_0}\left(\frac{\partial\theta_0}{\partial s_0} + \beta_0\frac{\partial\theta_0}{\partial n_0}\right)$$

and

$$A = \frac{2}{\beta_0 V_0^2}\left\{p_1\left[\left(\frac{\partial h}{\partial p}\right)_\rho + V_0 M_0^3\left(\frac{\partial a}{\partial p}\right)_\rho\right] + \rho_1\left[\left(\frac{\partial h}{\partial\rho}\right)_p + V_0 M_0^3\left(\frac{\partial a}{\partial\rho}\right)_p + \frac{\beta_0^2 V_0^2}{2\rho_0}\right]\right\}$$

$$B = \frac{2}{V_0^2}\left\{p_1\left(\frac{\partial h}{\partial p}\right)_\rho + \rho_1\left[\left(\frac{\partial h}{\partial\rho}\right)_p - \frac{V_0^2}{2\rho_0}\right]\right\}$$

In the foregoing equations, the characteristics coordinates $(\xi,\eta)$ as well as all quantities with zero subscripts are considered known from a solution of the axisymmetric flow for zero angle of attack. Therefore the five equations (9c, 10, 12c, 14a, and 14b) can be solved by usual difference methods for the perturbation quantities $p_1$, $\theta_1$, $\varphi_1$, $\rho_1$, $S_1$. Such a solution is subject to initial conditions and to boundary conditions at the shock and body surfaces. These conditions are listed next.

## Initial and Boundary Conditions

In the formulation of the foregoing equations it was not necessary to introduce any special orientation of the coordinate system (i.e., wind, body, or other axes). However, the form of initial and boundary conditions will vary with the choice of reference coordinate axes. From the standpoint of computational simplicity, there are some advantages associated with wind axes, and therefore this system is selected for the present problem.†

### *Initial conditions*

In order to begin the computation of the flow field about a general body, it is necessary to specify, along a line between the body and shock, values for the five perturbation quantities ($p_1$, $\theta_1$, $\varphi_1$, $\rho_1$, $S_1$), and also the shock-wave angle and position perturbations (these quantities are introduced in the shock conditions below). The required initial data may be obtained from cone solutions for pointed bodies and from "blunt-body" solutions if the body is not pointed. Cone data may be obtained from tabulated solutions[12, 13] or from a direct calculation of cone flow by the present method. For a blunt-nosed body, initial data are more difficult to obtain since yaw solutions are not generally available. (See Ref. 14 for a recent contribution to this problem.) However, for a spherical nose, the axisymmetric solution obtained by the inverse method[5, 15] can be applied to the yaw problem. For the spherical nose, initial values of all perturbation quantities are zero when expressed in terms of wind axes.

† To the contrary, however, it is often desirable to have results expressed in terms of body axes. Therefore, results obtained in terms of wind axes are usually transformed to body axes. The transformation equations, which depend on the axisymmetric flow field, are given in Refs. 10 and 11 for cone flow, and in Ref. 7 for more general flows. The results presented in the present paper are all converted to body axes.

### *Body conditions*

Two conditions that determine the flow angle $\theta = \theta_B$ and the entropy $S = S_B$ are available at the body surface. The corresponding conditions for the perturbation quantities are (in terms of wind axes)

$$(\theta_1)_B = -1 + (x - R_b)\frac{\partial\theta_0}{\partial r} - r\frac{\partial\theta_0}{\partial x} \tag{15}$$

$$(S_1)_B = K - [(x - R_b)\sin\theta_0 + r\cos\theta_0]\frac{dS_0}{dn_0} \tag{16}$$

where

$$K = \begin{cases} 0, & \text{spherical nose} \\ (S_1)_{\text{cone}}, & \text{pointed nose} \end{cases}$$

For the more general blunt-nosed body, the constant $K$ in Eq. (16) may not be zero.[14] In such a case, the specification of $K$ must come from the blunt-body solution.

### *Shock conditions*

When a body is yawed with respect to the freestream velocity, the shock wave will generally be displaced from its original position, and its angle will change. Consistent with the present first-order analysis, the shock radial position and the shock angle are written as

$$R(x, \Phi; \alpha) = R_0(x) + \alpha R_1(x)\cos\Phi \tag{17}$$

$$\sigma(x, \Phi; \alpha) = \sigma_0(x) + \alpha\sigma_1(x)\cos\Phi \tag{18}$$

The two variables $R_1$ and $\sigma_1$ introduced here are called the shock radial and angular perturbations. They are not independent, however (since $dR/dx = \tan\sigma$), but must satisfy the relation

$$(dR_1/dx) = \sigma_1 \sec^2\sigma_0 \tag{19}$$

Now for a given gas and for fixed upstream conditions ($p_\infty$, $\rho_\infty$, $V_\infty$), the shock relations depend only on the shock angle $\sigma$. That is,

$$\left.\begin{aligned} p &= p(\sigma) \\ \rho &= \rho(\sigma) \\ \theta &= \theta(\sigma) \end{aligned}\right\} \tag{20}$$

These shock relations may be written explicitly for a perfect gas, but are implicit for a real gas. Equations (20) can also be used to provide the derivatives of $p$, $\rho$, and $\theta$ with respect to $\sigma$, and these derivatives specify the perturbation variables immediately behind the shock wave. However, the displacement of the shock surface must also be accounted for. When this is done, the following shock conditions are obtained:

$$(p_1)_S = \sigma_1(dp/d\sigma) - R_1(\partial p_0/\partial r) \tag{21}$$

$$(\rho_1)_S = \sigma_1(d\rho/d\sigma) - R_1(\partial\rho_0/\partial r) \tag{22}$$

$$(\theta_1)_S = \sigma_1(d\theta/d\sigma) - R_1(\partial\theta_0/\partial r) \tag{23}$$

In these equations the derivatives with respect to $\sigma$ are obtained from Eqs. (20) and the derivatives with respect to $r$ are obtained from the corresponding axisymmetric solution.

One additional equation is needed for the crossflow angle $\varphi_1$ at the shock wave. This equation is obtained from the conservation of tangential momentum, and is given by

$$(\varphi_1)_S = \sigma_1\left[\frac{V_\infty}{V_0} - \cos\theta_0 + \left(\frac{x - R_b}{r}\right)\sin\theta_0\right] \tag{24}$$

This completes the specification of the equations and boundary conditions for the general body of revolution. The special case of conical flow is considered next.

### Specialization to Conical Flow

The equations and boundary conditions given previously for general bodies of revolution can be simplified somewhat for conical flow. In this case, all quantities depend only on the angular variable $\omega = \tan^{-1}(r/x)$, and the partial differential equations are reduced to ordinary equations. The compatibility relations Eqs. (14a) and (14b) become

$$\frac{\beta_0}{\rho_0 V_0^2}\frac{dp_1}{d\omega} = \frac{M_0 r}{2\sin\omega}\left[\frac{(F_1 - G)}{E_1} - \frac{(F_2 - G)}{E_2}\right] \quad (25a)$$

$$\frac{d\theta_1}{d\omega} = \frac{M_0 r}{2\sin\omega}\left[\frac{(F_1 - G)}{E_1} + \frac{(F_2 - G)}{E_2}\right] \quad (25b)$$

where

$$E_1 = \cos(\omega - \theta_0) - \beta_0 \sin(\omega - \theta_0)$$

$$E_2 = \cos(\omega - \theta_0) + \beta_0 \sin(\omega - \theta_0)$$

and the terms $F_1$, $F_2$, and $G$ are unchanged [see Eqs. (14)]. Equation (9c) for the crossflow-angle perturbation is transformed to

$$\frac{d\varphi_1}{d\omega} = \left[\frac{1}{\rho_0 V_0^2}\frac{dp_0}{d\omega} + \frac{\sin\theta_0}{\sin\omega\sin(\omega - \theta_0)}\right]\varphi_1 - \frac{p_1}{\rho_0 V_0^2 \sin\omega \sin(\omega - \theta_0)} \quad (26)$$

and Eqs. (10–12) are unchanged. Since the axisymmetric conical flow is isentropic (i.e., $dS_0/dn = 0$), Eq. (10) states that the entropy perturbation is a constant everywhere in the shock layer. Therefore, its value must be given by Eq. (12c) in terms of pressure and density perturbations at the shock. Thus,

$$S_1 = \left(\frac{\partial S}{\partial p}\right)_\rho (p_1)_S + \left(\frac{\partial S}{\partial \rho}\right)_p (\rho_1)_S = \text{const} \quad (27)$$

Finally, the flow-angle perturbation at the body [Eq. (15)] is reduced to

$$(\theta_1)_B = -2 \quad (28)$$

Equation (27) implies that the entropy varies circumferentially (i.e., $S = S_0 + \alpha S_1 \cos\Phi$), which contradicts the usual condition that the body surface should have a constant value of entropy for all values of $\Phi$. The contradiction is resolved by allowing for a very thin "vortical" layer next to the cone surface.[8] Across this layer the pressure and flow angle are constant, but the entropy, density, and velocity change abruptly.‡ Equation (27) is therefore the correct condition for the flow outside the vortical layer. However, the vortical layer is much thinner than the viscous boundary layer, and therefore the results obtained from the present equations provide the pertinent conditions for a boundary-layer analysis.[18]

The shock conditions for conical flow may be written

$$(p_1)_S = \sigma_1[(dp/d\sigma) - (dp_0/d\omega)] \quad (29)$$

$$(\rho_1)_S = \sigma_1[(d\rho/d\sigma) - (d\rho_0/d\omega)] \quad (30)$$

$$(\theta_1)_S = \sigma_1[(d\theta/d\sigma) - (d\theta_0/d\omega)] \quad (31)$$

$$(\varphi_1)_S = \sigma_1[(V_\infty/V_0) - \cos\theta_0 + \sin\theta_0 \cot\sigma_0] \quad (32)$$

Since the shock-angle perturbation $\sigma_1$ is unknown a priori, numerical calculations for the cone problem are most easily handled in an inverse manner. One begins at the shock wave with an arbitrary value for $\sigma_1$ and proceeds stepwise to the body. Because of the linearity of the problem, all computed values (as well as $\sigma_1$) are then adjusted so as to satisfy Eq. (28) on the body surface.

‡ The details of the vortical layer have been studied in Refs. 16 and 17 for both first- and second-order perturbations.

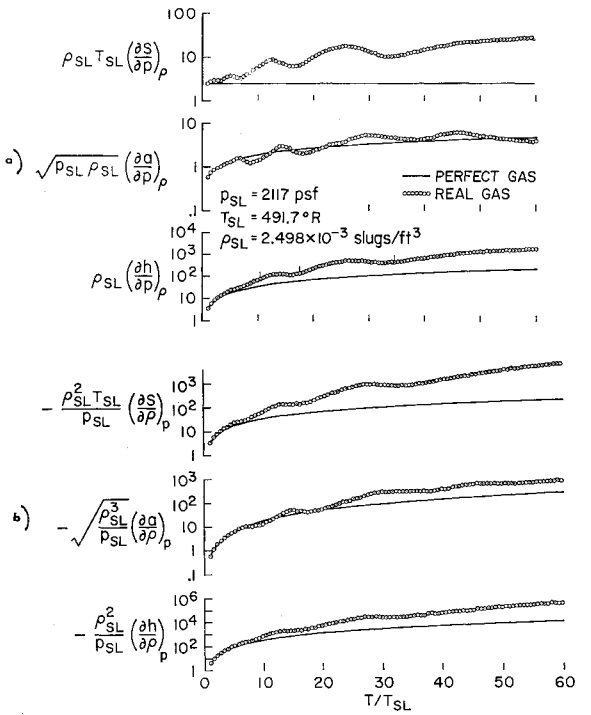


**Fig. 2 Thermodynamic derivatives for equilibrium air; a) derivatives at constant density and b) derivatives at constant pressure.**

This completes the specification of the problem, and attention is now directed to those aspects of the equations affected by the gas properties.

### Discussion of the Equations

Since the results presented below are intended to illustrate the effects of equilibrium gas properties, it is pertinent at this point to review the equations from this standpoint. The gas properties enter the forementioned perturbation equations in three ways. First, the coefficients of the perturbation variables contain quantities that depend on the axisymmetric solution and these quantities are affected by the state relations. Second, the six thermodynamic derivatives in Eqs. (12) enter into the terms $A$ and $B$ in Eqs. (14), and in Eq. (10). Finally, the shock conditions Eqs. (21–23), contain derivatives with respect to the shock angle $\sigma$.

The present formulation of the problem is completely general in that it does not depend on a particular gas model. It is only necessary that the enthalpy, speed of sound, and entropy be given in terms of pressure and density. This approach was made possible through the efforts of Harvard Lomax of Ames Research Center who provided the computer subroutines that give the necessary state properties. The properties are determined from curve fits to the tabulated data of Hilsenrath and Beckett.[19] The computer subroutines that provide the curve fits optimize the access time for fixed error. Curve fits used for the present results are in error by a maximum of 5% and by less than 1% for most conditions.[5] As a result of having the state properties conveniently specified in computer language, the partial derivatives required for the present problem are easily obtained by numerical methods. The result of this process is illustrated in Fig. 2, which shows the six partial derivatives for one atmosphere of pressure and for a range of temperatures. These derivatives are normalized with the sea-level values of pressure, temperature, and density so as to make them dimensionless. As the temperature is increased, the real-gas curves deviate from the perfect-gas curves as a result of the dissociation and ionization of the gas. These deviations are large in some cases and one might, therefore, expect some effect on the flow field.

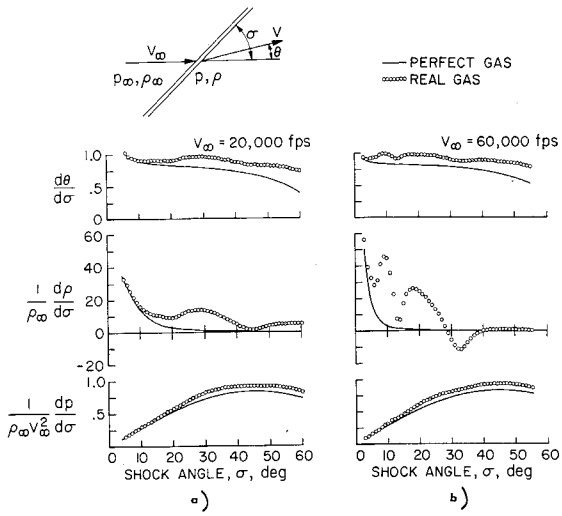


**Fig. 3 Shock-wave derivatives for air at 100,000-ft alt; a) $V_\infty$ = 20,000 fps and b) $V_\infty$ = 60,000 fps.**

Numerical methods were also applied to the shock-wave equations in order to calculate the derivatives which appear in the shock-wave boundary conditions. Some typical results for these derivatives, normalized with freestream conditions, are shown in Fig. 3. It is seen that the density is the quantity most affected by the dissociation and ionization of the gas. For a flight velocity of 60,000 fps [Fig. 3b], the density derivative changes sign for shock angles near 35°. These negative slopes also appear in the results of Ref. 20 and will be seen to have an appreciable effect on the flow-field results presented next.

## Results

In order to illustrate some of the features of the perturbation flow field for an equilibrium gas, attention is directed to solutions for some particular body shapes. The results of these solutions are presented in Figs. 4–8 in terms of body axes.

### Cones

Because of their simplicity, solutions for pointed cones are particularly useful for investigating major trends in the results. Thus, for example, cone angle and altitude can be fixed, and velocity can be varied to produce varying degrees of dissociation in the shock layer. Figure 4 shows such results in which the flight velocity is varied from 5000 to 75,000 fps. Of the variables studied, the surface pressure perturbation is least affected by gas properties. It varies by less than 2% over the entire velocity range. On the other hand, the density perturbation is changed greatly. The negative

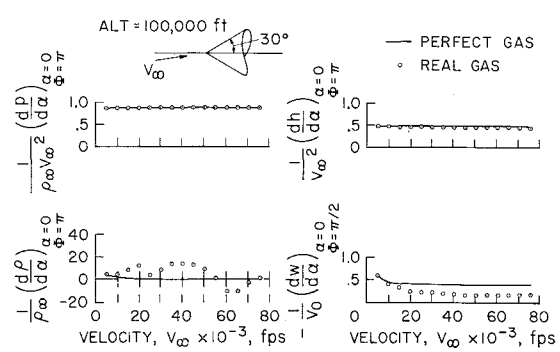


**Fig. 4 First-order perturbation parameters at the surface of a 30° cone at an altitude of 100,000 ft.**

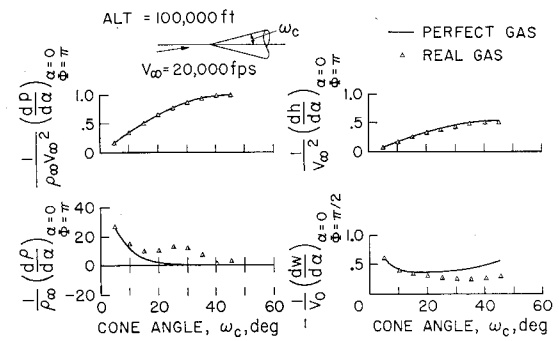


**Fig. 5 First-order perturbation parameters at the surface of cones for a velocity of 20,000 fps and an altitude of 100,000 ft.**

density perturbation between flight velocities of approximately 55,000 to 73,000 fps is a curious result that will be discussed below; it implies a decrease in density along the windward rays of a yawing cone. The enthalpy perturbation is affected by the gas properties only slightly more than the pressure perturbation. The crossflow velocity perturbation decreases nearly monotonically and reaches 40% of the perfect-gas value at about 50,000 fps.

The cause of the large variations of the density perturbation can be illustrated more clearly by the results for different cone angles at fixed flight conditions. Such results are shown in Fig. 5 for a flight velocity of 20,000 fps at an altitude of 100,000 ft and for cone angles from 5° to 45°. For the large flight velocities considered, the shock layer is very thin and the shock angle is nearly equal to the cone angle. Therefore, the density curve in Fig. 5 may be compared directly with that for the shock-wave derivative ($d\rho/d\sigma$) in Fig. 3a. It is noted that the variation of the surface density perturbation follows that of the shock derivative. This implies that the large changes in the density perturbation are primarily due to the shock conditions. By means of this conclusion, the cause of the previously mentioned negative density perturbation is easily explained. It is well known that the equilibrium density rise across shock waves can, as shown in Fig. 3b, decrease with increasing shock angle (see, also, Ref. 20). For these flight conditions, the first-order variation of the surface density on the windward side of the cone is to decrease with increasing angle of attack.

The results in Figs. 4 and 5 show the separate, or independent effects of flight velocity and cone angle. However, according to hypersonic similarity concepts, one would expect that these results might depend only on the component of velocity normal to the cone surface. In Ref. 3, such a similarity was illustrated for unyawed cones. The reason

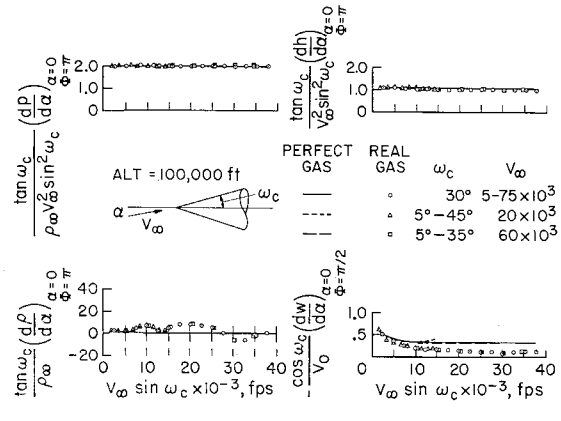


**Fig. 6 Correlation of first-order perturbation parameters at the surface of cones at hypersonic speeds and at an altitude of 100,000 ft.**

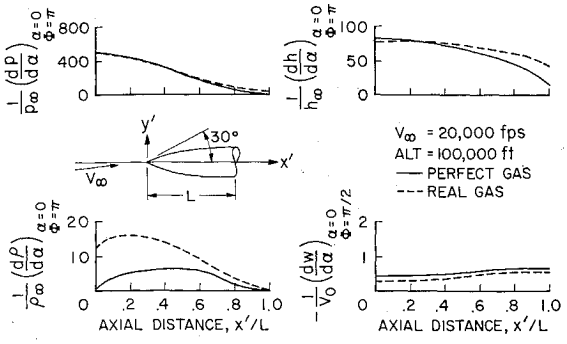


**Fig. 7 Perturbation variables on the surface of a 30° ogive for a flight velocity of 20,000 fps at 100,000-ft alt.**

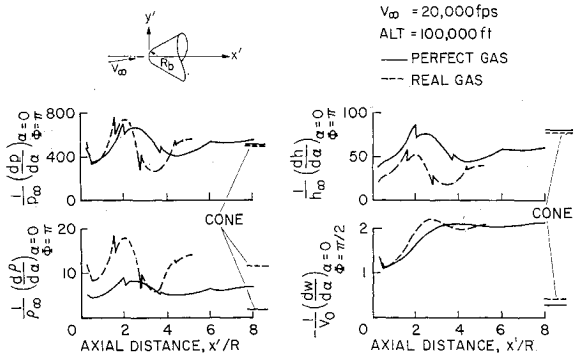


**Fig. 8 Perturbation variables on the surface of a 30° sphere-cone for a flight velocity of 20,000 fps at 100,000-ft alt.**

the cone-flow results are correlated in this way is, apparently, that the shock layer is very thin at high velocities, and the changes in pressure and flow inclination are very small across this layer. The flow field therefore depends primarily on the shock conditions and these conditions depend only on the freestream pressure and density and on the component of velocity normal to the wave. Furthermore, since the cone and wave angles are nearly the same, the velocity component normal to the cone surface may be used as the correlating parameter.

In the present case, where the shock conditions involve derivatives with respect to angle of attack [Eqs. (29–31)], the tangential component of velocity $V_\infty \cos\omega_c$ also enters as a parameter. The results of Figs. 4 and 5 have been modified to account for this dependence and have been replotted in Fig. 6 as a function of $V_\infty \sin\omega_c$. Results for several cones at 60,000 fps have also been added to this figure. It is seen that the results correlate very well. These curves should therefore apply to any other combination of velocity and cone angle, provided the shock wave is attached and the velocity is large enough. For other altitudes, however, a different set of curves must be obtained.

## General Bodies

The cone solutions presented in the previous section demonstrated some basic features of real-gas flows. The question remains, however, as to whether these features of conical flows apply to more general flows. In order to study this question, selected results for a pointed ogive and for a spherically tipped cone are presented next. These results will be confined to only one set of flight conditions and will demonstrate how the perturbation quantities vary along the body surface for perfect- and equilibrium-air flows.

### *Ogive*

Figure 7 shows the pressure, density, enthalpy, and crossflow-velocity perturbations for an ogive with a 30° apex angle. The flight velocity is 20,000 fps and freestream conditions correspond to 100,000-ft alt. Initial conditions for the ogive calculations are obtained from the solution for the tangent cone to the ogive at $x/L = 0.01$. It is seen in Fig. 7 that the surface pressure perturbation is relatively unaffected by the gas properties, whereas the density and enthalpy perturbations are changed appreciably. The density perturbations for real and perfect gases differ widely at the nose but approach the same value near the base of the ogive. Conversely, the enthalpy perturbations are nearly the same at the nose but the real-gas result is higher by a factor of 2 near the base. The crossflow-velocity perturbations from the real- and perfect-gas solutions differ by a nearly constant amount over the entire length of the ogive.

### *Sphere-cone*

Similar results are shown in Fig. 8 for a 30° sphere-cone at 20,000 fps flight velocity and at an altitude of 100,000 ft. In this case, however, some new features are noted. First, it is seen that the crossflow-velocity perturbation does not approach the pointed-cone value whereas the pressure perturbation does. This indicates the development of the vortical layer which was previously mentioned in connection with the cone boundary conditions. At the surface of the sphere-cone body, the entropy perturbation is zero [Eq. (16)], while its value just off the body must approach the pointed-cone value.

The second feature to be noted in Fig. 8 is that the pressure perturbation exhibits discontinuities for both real- and perfect-gas flows. They arise from the fact that the gradients of the axisymmetric solution are discontinuous as a result of the discontinuous curvature at the sphere-cone juncture. The characteristic from this point reflects repeatedly between shock and body surfaces, and thereby propagates the disturbance downstream. The locus of this characteristic curve controls the way in which the initially spherical flow adjusts to the conical boundary. This explains the sizable difference in the pressure perturbation curves for real and perfect gases. For the real-gas flow, the bow shock wave lies closer to the body and a characteristic from the body reflects from the bow wave and back to the body more quickly than for a perfect-gas flow (see Fig. 9). The result is that the hump in the pressure perturbation curve is closer to the nose for the real-gas flow and the pressure perturbation approaches the conical flow value more quickly than it does for perfect gas (but approaches nearly the same value in either case). For sphere-cones with certain values of the ratio of body length to nose radius, the forward shift in the pressure perturbation curve can have an adverse effect on the stability. For example, in the present case for a body length of 3.5 nose radii, the center

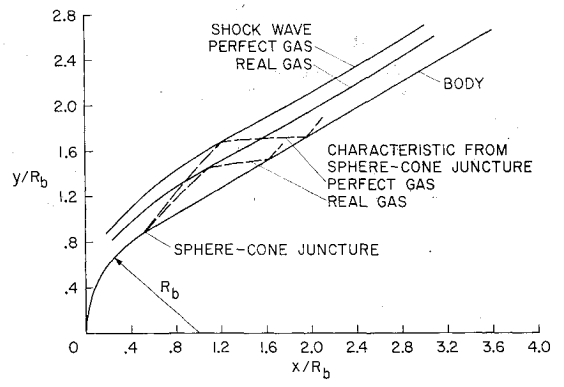


**Fig. 9 Comparison of shock shapes for real- and perfect-gas flow over a 30° sphere-cone.**

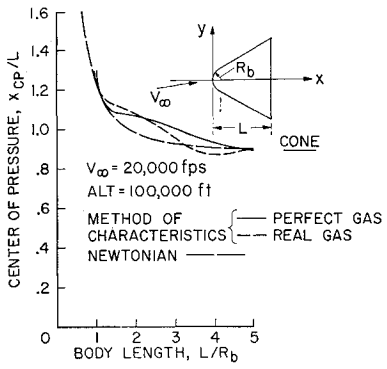


**Fig. 10 Comparison of the center of pressure for real- and perfect-gas flow over a 30° sphere-cone.**

of pressure is shifted forward about 7% of the body length as a result of the real-gas effects (Fig. 10).

This change in the flow pattern for a real gas is caused primarily by changes in the axisymmetric flow field. For pointed bodies, it was found that the most significant real-gas effects were due to the shock boundary conditions that caused a large change in the density perturbation. The same is true for the blunted body, as is evident from the density perturbation shown in Fig. 8. However, as seen already, for the sphere-cone an additional change to the flow field is caused by the decreased shock-layer thickness in a real gas.

## Concluding Remarks

The effect of equilibrium thermodynamics on the perturbation flow field for selected bodies of revolution has been investigated with a linearized characteristics method which has certain inherent limitations. It seems appropriate, therefore, to conclude with a few words about the applicability of the results that have been presented.

Although the linearized method yields exact numerical results for the initial slope of flow variables, the second-order, or quadratic, term in the series expansion can, under some conditions, exceed the linear term even for small angles of attack. The problem of evaluating the higher-order terms is a difficult one for general body shapes, and requires additional effort. However, preliminary estimates have been made which indicate that the second-order term is usually negligible when the local body slope is greater than the angle of attack. Accordingly, the results shown for the 30° cone are expected to be quite reliable for moderate angles of attack (this conclusion is also verified by experiment[7]). Near the base of the ogive, where the body slope is small, the results shown should be treated with some caution since the higher-order terms may become dominant there. It should, however, be noted that the second-order pressure term adds to the axial force, but not to the normal force.[12] Therefore, the center of pressure is exact to second-order in angle of attack.

The final point to be mentioned is in regard to the discontinuous jumps in the perturbation variables (Fig. 8) which are often viewed with some dismay. These jumps represent the exact inviscid solution in the limit as the angle of attack tends to zero; they necessarily follow from the fact that the gradients of the axisymmetric solution are discontinuous as a result of the change of curvature at the juncture between the spherical nose and the conical afterbody. For application to nonzero angles of attack, there is a small region around the discontinuity [of the order, $\Delta x = 0(\alpha)$] in which the assumed series expansion is not valid. In this region, a continuous transition curve must connect the two branches so as to provide for a continuous variation of the actual flow variables while allowing discontinuous gradients. The results obtained by neglecting the transition curve are usually sufficiently accurate for most applications and, therefore, the importance of the discontinuities should not be overemphasized.

## References

[1] Gravalos, F. G., Edelfelt, I. H., and Emmons, H. W., "The supersonic flow about a blunt body of revolution for gases at chemical equilibrium," *Proceedings IX International Astronautical Congress* (Springer-Verlag, Wien, Austria, 1959), Vol. 1, pp. 312–332.

[2] Romig, M. F., "Application of the hypersonic similarity rule to conical flow of dissociated air," Aero/Space Eng. **18,** 56–59, 75 (March, 1959).

[3] Feldman, S., "Hypersonic conical shocks for dissociated air in thermodynamic equilibrium," Jet Propulsion **27,** 1253–1255 (1957).

[4] Zienkiewicz, H. K., "Flow about cones at very high speeds," Aeronaut. Quart. **8,** 384–394 (1957).

[5] Lomax, H. and Inouye, M., "Numerical analysis of flow properties about blunt bodies moving at supersonic speeds in an equilibrium gas," NASA TR R-204 (July 1964).

[6] Brong, E. A. and Edelfelt, I. H., "A flow field about a spherically blunted body of revolution at small yaw in a hypersonic stream," IAS Paper 62-181 (1962).

[7] Rakich, J. V., "Numerical calculation of supersonic flows of a perfect gas over bodies of revolution at small angles of yaw," NASA TN D-2390 (July 1964).

[8] Ferri, A., "Linearized characteristics methods," *General Theory of High Speed Aerodynamics,* edited by W. R. Sears (Princeton University Press, Princeton, N. J., 1954), pp. 657–668.

[9] Stone, A. H., "On supersonic flow past a slightly yawing cone," J. Math. Phys. **27,** 67–81 (April 1948).

[10] Van Dyke, M. D., Young, G. B. W., and Siska, C., "Proper use of the M.I.T. tables for supersonic flow past inclined cones," J. Aerospace Sci. **18,** 355–356 (1951).

[11] Roberts, R. C. and Riley, J. D., "A guide to the use of the MIT cone tables," J. Aerospace Sci. **21,** 336–342 (1954).

[12] Staff of the Computing Section, "Tables of supersonic flow around yawing cones," Massachusetts Institute of Technology TR 3 (1947).

[13] Sims, J. L., "Tables for supersonic flow around right circular cones at small angle of attack," NASA SP-3007 (1964).

[14] Swigart, R. J., "A theory of asymmetric hypersonic blunt-body flows," AIAA J. **1,** 1034–1042 (1963).

[15] Van Dyke, M. D. and Gordon, H. D., "Supersonic flow past a family of blunt axisymmetric bodies," NASA TR R-1 (1959).

[16] Cheng, H. K., "Hypersonic flows past a yawed circular cone and other pointed bodies," J. Fluid Mech. **12,** 169–191 (February 1962).

[17] Munson, A. G., "A uniformly valid solution for the flow over an inclined cone using the method of matched asymptotic expansions," Stanford Univ. Dept. of Aeronautics and Astronautics, Rept. 187 (April 1964).

[18] Moore, F. K., "Laminar boundary layer on a circular cone in supersonic flow at a small angle of attack," NASA TN 2521 (1951).

[19] Hilsenrath, J. and Beckett, C. W., "Tables of thermodynamic properties of argon-free air to 15,000°K," Arnold Engineering Development Center, AEDC TN 56-12 (September 1956).

[20] Feldman, S., "Hypersonic gas dynamic charts for equilibrium air," Avco-Everett Research Lab., Research Rept. 40 (January 1957).